Hydrogen Storage in Porous Transition Metals Nitroprussides

L. Reguera,[†] J. Balmaseda,[‡] C.P. Krap,[||] and E. Reguera*[,||,§]

Facultad de Quimica and Instituto de Ciencia y Tecnología de Materiales, Universidad de La Habana, Cuba, Departamento de Polímeros, Instituto de Investigaciones en Materiales, Universidad Nacional Autónoma de México (UNAM), México, D.F. C.P. 04510, and Centro de Investigación en Ciencia Aplicada y Tecnología Avanzada-Unidad Legaria, Instituto Politécnico Nacional, México, D.F

Received: March 5, 2008; Revised Manuscript Received: April 23, 2008

Transition metals nitroprussides form a family of porous molecular materials with relative wide diversity of crystalline structures and also of porous network topologies. These features make nitroprussides interesting cyanometallates-based materials where the role of structural factors on the hydrogen storage can be evaluated. The hydrogen adsorption was studied in T[Fe(CN)$_5$NO] with T = Mn, Fe, Co, Ni, Cu, Zn, and Cd; in a series of mixed compositions, Co$_{1-x}$T$_x$[Fe(CN)$_5$NO] with T = Mn, Fe, Ni, Zn, and Cd; and in Cu$_{0.55}$Ni$_{0.45}$[Fe(CN)$_5$NO]. The largest hydrogen storage capacity was found for Ni[Fe(CN)$_5$NO], 2.54 mol/mol (1.85 wt %) at 75 K and 850 Torr. The hydrogen adsorption in nitroprussides shows a marked dependence on the properties of the metal (T) situated at the cavity surface. The electrostatic interaction between the hydrogen molecule quadrupole moment and the electric field gradient at the cavity surface appears to be the main driving force for the hydrogen adsorption, without discarding a possible direct interaction of H_2 with the metal (T). In structures with narrow channels (Mn, Cd), pronounced kinetic effects for the H_2 adsorption isotherms are observed, which were ascribed to a strong and localized interaction between the H_2 molecule and the metal at the cavity surface. The pore accessibility and the pore volume were evaluated from CO_2 adsorption isotherms. The free volume for all the compositions are accessible to the CO_2 molecule. The CO_2 stabilization within the cavities is also dominated by the electrostatic interaction. All the samples were previously characterized using X-ray energy-dispersed spectroscopy, X-ray diffraction, thermogravimetry, and infrared and Mössbauer spectroscopies.

1. Introduction

Nowadays, about 80% of the consumed energy comes from combustion of fossil fuels derivatives, energy source whose availability will be limited in the near future. The combustion of fossil fuels and their derivatives are also partially responsible for the emission of greenhouse gases and for the related global warming and climate changes. Among the alternatives to fossil fuels derivatives as energy sources, for use in automotive vehicles, for instance, combustion of hydrogen has being considered, due to its high caloric value (572 kJ/mol) and environmentally compatible byproduct (water).[1] Hydrogen has too low critical temperature (32.7 K) to be handled in liquid state for practical applications such as combustible. From these facts, a challenge for the development of a hydrogen-based energy technology is the availability of appropriate hydrogen storage media. The established target (2010 US DOE targets), in that sense, is 6 wt % for a reversible process and relatively short storage−release times.[2] To date, the highest hydrogen storage capacity in materials has been reported for chemical and metal hydrides,[3] with some of them above that target.[4] However, the desorption process of hydrogen stored as hydrides usually requires relatively high temperatures of heating (>500 K) and this storage method is not always reversible.[5] An attractive option for a reversible process is the storage through physical adsorption in porous materials; however, to date, the reported gravimetric density of hydrogen adsorbed at atmospheric pressure remains below the target of 6 wt %,[6] suggesting that more basic studies are required in order to increase the hydrogen storage density in porous solids. Several families of porous materials have been evaluated in that sense, among them, carbon-based solids,[7,8] zeolites,[9,10] and metal organic frameworks.[11–13] More recently, porous coordination polymers, of Prussian blue type, have received certain attention as prototype materials for hydrogen storage;[14–19] among them, cobalt and nickel nitroprussides have the highest reported hydrogen adsorption efficiency for a porous coordination polymer-based material, 1.68 wt %.[17] Cobalt and nickel nitroprussides are only two members of this family of coordination compounds, which shows a relative wide diversity of crystalline structures and also of topologies for the porous network.[20] These features make nitroprussides an interesting family of porous molecular materials that deserves to be evaluated for hydrogen storage, particularly to obtain information on the role of the pore topology on the hydrogen adsorption. In addition, for the anhydrous phases of this family of compounds the assembling metal (T) is always found with an unsaturated coordination sphere and is located at the cavities' surface. As for the hydrogen interaction with such metal centers, a certain role for the H_2 adsorption in porous solids has been attributed.[14–19,21]

In this contribution, the results obtained from a study on hydrogen storage in the family of transition metals nitroprussides, T[Fe(CN)$_5$NO] with T = Mn, Fe, Co, Ni, Cu, Zn, and Cd, including a series of mixed compositions,

* To whom correspondence should be addressed. E-mail: ereguera@yahoo.com.
[†] Universidad de La Habana.
[‡] Universidad Nacional Autónoma de México.
[||] Centro de Investigación en Ciencia Aplicada y Tecnología Avanzada-Unidad Legaria.
[§] Instituto de Ciencia y Tecnología de Materiales.

10.1021/jp801955p CCC: $40.75
Published on Web 06/20/2008

$Co_{1-x}T_x[Fe(CN)_5NO]$ with T = Mn, Fe, Ni, Zn, and Cd, and $Cu_{0.55}Ni_{0.45}[Fe(CN)_5NO]$, are reported. These mixed compositions were studied in order to shed light on the role of the metal (T) situated at the pore surface on the material's ability for hydrogen adsorption. All the studied samples were characterized by X-ray energy-dispersed spectroscopy (EDS), X-ray diffraction (XRD), thermogravimetry (TG), infrared (IR) and Mössbauer spectroscopies, and CO_2 adsorption data. The mixed metals nitroprussides were prepared and characterized for all the possible combinations of the involved T metals. From the CO_2 adsorption data, information on the material pore volume and pore accessibility was obtained.

2. Experimental Section

The samples were prepared by mixing 0.01 M aqueous solutions of sodium nitroprusside ($Na_2[Fe(CN)_5NO]\cdot 2H_2O$) and of sulfates of the involved divalent transition metals (T = Mn, Fe, Co, Ni, Cu, Zn, Cd). To obtain the mixed compositions, $T^A_{1-x}T^B_x[Fe(CN)_5NO]\cdot xH_2O$, the precipitation process was carried out from equimolar aqueous solutions of the metals T^A and T^B. For this last series, an excess of the metals solution with respect to sodium nitroprusside was used in order to avoid precipitation of the two phases. The formed precipitates were then separated by centrifugation, followed by successive washing with distilled water, and finally by air-drying until they had constant weight. The reagents used were analytical grade from Sigma-Aldrich. The nature of the obtained samples was established from EDS, XRD, IR, and Mössbauer data. The hydration degree (number of water molecules per formula unit) was estimated from TG curves.

IR spectra were recorded in an FT-IR spectrophotometer (Genesis Series from Atti Matson) using the KBr pressed disk technique. XRD powder patterns were obtained with Cu Kα radiation in an HZG-4 diffractometer, and their preliminary evaluation was carried out using the program Dicvol.[22] The cell contraction on the crystal water removal was evaluated from XRD powder patterns recorded at the X10B beamline of the LNLS synchrotron radiation facility (Campinas, Brazil). TG curves were collected from 25 to 300 °C, under a N_2 flow (100 mL/min) using a TA instrument thermo-balance (TGA 2950 model) operated in the high-resolution mode. The crystallite size was estimated from the obtained XRD data using the Scherrer equation,[23] removing the instrumental broadening.

The CO_2 and H_2 adsorption isotherms were recorded using ASAP 2010 and 2020 analyzers (from Micromeritics), respectively. Sample tubes of known weight were loaded with an appropriate amount of sample, ~100 mg for CO_2 and 40 mg for H_2, and were sealed using TranSeal. In this family of materials the most reliable H_2 adsorption data, using an optimal measurement time, were obtained with that relative small amount of samples. Previous to CO_2 and H_2 adsorption, the samples were degassed on the ASAP analyzer using a heating rate of 5 °C/min and then maintained at the dehydration temperature indicated by the TG curve until a stable outgas rate below 1 μm Hg was obtained. This process usually requires 24 h of degassing. The degassed sample and sample tube were weighed and then transferred back to the analyzer (with the TranSeal to prevent exposure of the sample to air). After volume measurement with He, the degassing was continued for 24 h at 80 °C in the sample port. Measurements were performed at 273 K for CO_2 using an ice−water bath and at 75 and 85 K for H_2 in liquid N_2 and Ar baths, respectively. These relatively low temperatures for liquid N_2 (75 K) and Ar (85 K) are related to the local atmospheric pressure, 586 Torr.

The CO_2 adsorption data were evaluated according to the Dubinin−Astakhov (DA) equation,[24]

$$n_{ad} = n_p \cdot \exp\left\{-\left[\frac{RT}{E_0}\ln(P_r^{-1})\right]^n\right\} \quad (1)$$

where n_{ad} is the amount adsorbed at a relative pressure $P_r = P_{eq}/P_v$, n_p is the limiting amount filling the micropores, E_0 is the characteristic energy, n is the heterogeneity parameter, R is the universal gas constant, and T is the temperature. Because the CO_2 adsorption data were collected up to 760 Torr, at a temperature close to the critical temperature for this adsorbate (304 K), the obtained isotherms only contain points at relative pressures below 0.03, far from the saturation region. In such conditions the correlation between DA model parameters for nonlinear least-squares fitting algorithms leads to nonreliable n_p values. From this fact, the n_p value was estimated using the more general Langmuir−Freundlich (LF) equation based on the vacancy solutions theory,[25]

$$P_{eq} = P_{0.5}\left(\frac{n_{ad}}{n_p - n_{ad}}\right)^g \quad (2)$$

where $P_{0.5}$ is the equilibrium pressure at $n_p/2$, g is the osmotic coefficient related to ideality of solution, and the remaining parameters have the same meaning as in DA equation. Then, once the value of n_p is known, from eq 1, the values of E_0 and n are calculated. Details on this combined application of DA and LF models for the evaluation of adsorption data have been reported elsewhere, including the nonlinear fitting algorithm.[26] The pore volume was estimated by multiplying the obtained n_p value by the reported molar volume for liquid CO_2 (42.9 mL/mol).[27]

Within the DA model formalism, the adsorption potential [$A(-\Delta G)$] can be estimated directly from the obtained adsorption isotherm according to eq 3.[24,27,28]

$$A = RT\ln(P_r^{-1}) \quad (3)$$

For the CO_2 adsorption data, where the DA model was applied, the variation for the adsorption potential (A) on the fractional volumetric pore filling θ (n_{ad}/n_p) provided information on the guest−host interaction involved in the adsorption phenomenon.

The hydrogen adsorption isotherms were evaluated according to eq 2 to estimate the limit capacity of micropores (n_p) and the osmotic coefficient (g) value. A previous study on the hydrogen adsorption in porous cyanometallates indicates that the value of g can be used as a sensor for the strength of the guest−host interaction.[29] The heat of adsorption (ΔH_{ads}) was obtained by the isosteric method from isotherms recorded at N_2 and Ar baths and then using a variant of the Clasius−Clapeyron equation to calculate the ΔH_{ads} value according to eq 4.[30]

$$\ln\left(\frac{P_1}{P_2}\right) = \frac{\Delta H_{ads}}{R}\frac{T_2 - T_1}{T_1 T_2} \quad (4)$$

3. Results and Discussion

3.1. Nature of the Samples to be Studied. *$T[Fe(CN)_5NO]\cdot xH_2O$ Series.* The estimated metals atomic ratio (Fe/T) found from EDS spectra for simple nitroprussides was close to 1:1, in accordance with their nominal formula unit, $T[Fe(CN)_5NO]\cdot xH_2O$. The XRD powder patterns for this series correspond to the reported crystal structures for the hydrated phases of divalent transition metals nitroprussides: Mn and Cd (orthorhombic, *Pnma*); Cu (orthorhombic, *Amm*2); Fe, Co, and

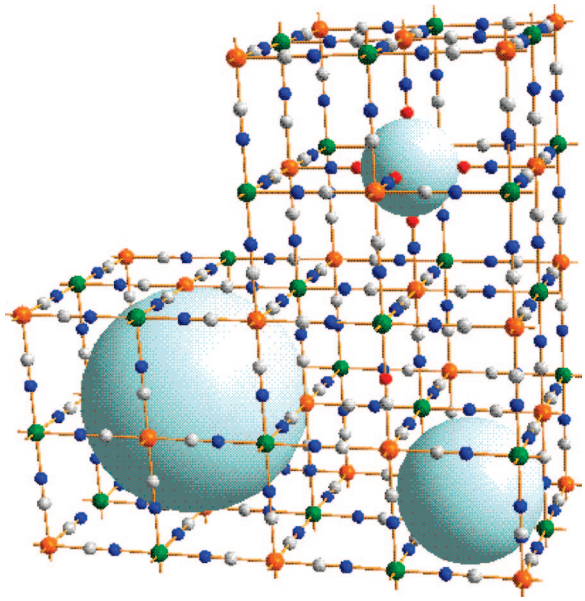

Figure 1. Porous framework of cubic nitroprussides. The largest sphere corresponds to a pore generated by a vacancy of the building block, $[Fe(CN)_5NO]$; the intermediate size sphere represents the interstitial free spaces; and the third sphere (of smallest size) corresponds to the free space related to a vacancy for the assembling metal (the NO bound cage).

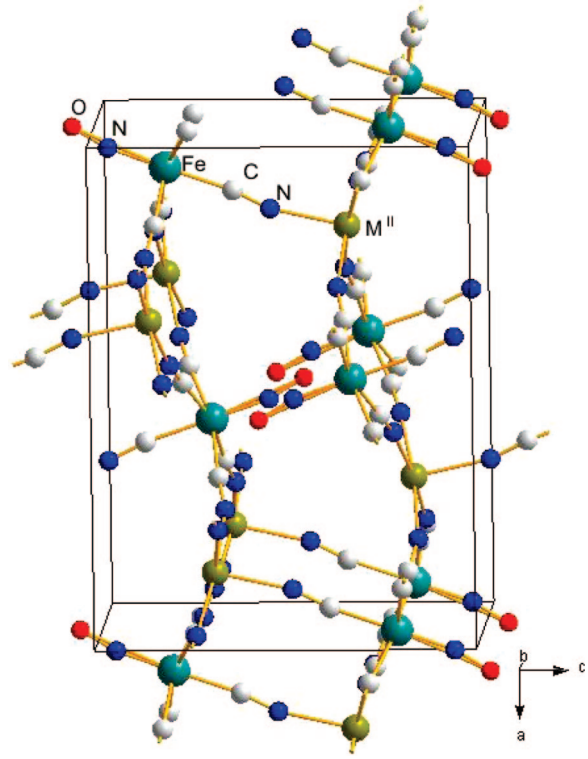

Figure 2. Atomic packing within the unit cell for orthorhombic (*Pnma*) anhydrous nitroprussides. When the crystal water is removed, a system of trapezoidal narrow channels appears. At the channel surface, metal atoms with an unsaturated coordination sphere are located.

Ni (cubic, $Fm\bar{3}m$); and Zn (rhombohedral, $R\bar{3}$).[31–33] For adsorption studies these compounds must be dehydrated in order to liberate the available free space in the structure from water molecules. The crystal structures for the anhydrous phases of this series of compounds are known.[33–35] Except for Cu, upon water removal the material framework is preserved with certain cell contraction, which for cubic phases is the largest, and amounts to 2% of cell volume reduction.[34] For Cu, the water removal leads to a structural transformation to form a tetragonal phase also of porous nature.[33] In Figures 1–4 the porous networks of this family of materials as anhydrous phases are illustrated. In the cubic phases, the building blocks $[Fe(CN)_5NO]$ are accommodated in such a way that six unlinked ends—the NO group—are oriented toward a metal vacant site, creating a hydrophobic cavity of ca. 4 Å (Figure 1).[34] To preserve the charge neutrality, that vacancy for the metal forces to the existence of a vacancy for the building block, $[Fe(CN)_5NO]$. The block vacancy originates a larger cavity of ca. 8.5 Å with hydrophilic character. These free spaces form a three-dimensional (3D) network of cavities that remain communicated by the interstitial free spaces, of ca. 4.5 Å of diameter (Figure 1). At the surface of the largest cavity, six T atoms with an incomplete coordination sphere are found. In the hydrated phases these available coordination sites are occupied by coordinated waters. For the orthorhombic phases (Mn, Cd), neighboring building blocks are accommodated maintaining antiparallel their NO groups, whereas the axial cyanide behaves as a bridge group shared by the two metal centers (Figure 2).[35] From such an arrangement of building units, a ripple sheet framework results. In the formed structure a system of trapezoidal narrow channels is found, with a transversal cross section of about 4.5 Å. These channels have a hydrophilic surface because of the unsaturated coordination sphere for the metal situated at the channels surface. For zinc, the building units are accommodated in such a way that six NO groups of neighboring blocks form a hexagonal opening of about 4 Å (diameter).[35] Two of these NO openings delimit an ellipsoidal cavity of about 15 × 10.35 Å (Figure 3). Six Zn atoms are situated on the surface of this cavity. The unit cell volume contains three of such cavities. Anhydrous copper nitroprusside (tetragonal $I4mm$) has a 3D network of communicated perpendicular narrow channels, one of them—the U-shaped channel—with a line of NO groups at its center (Figure 4).[33] The unlinked NO group is found at only ca. 2.9 Å from the copper atom, which probably limits the metal interaction with guest species to be adsorbed. From this fact, this compound probably behaves as a porous cyanometallate with only interstitial voids as available free spaces.

The crystallite size for the obtained powders depends on the involved metal (Table 1). A metal with a strong interaction with the CN group, such as Ni^{2+}, usually leads to powders of small crystallite size.[34] Because the metal is situated at the cavities surface where it has mixed coordination environment, the generated local strains do not favor the crystal growth until relatively large size.

The structural characterization of this series was completed from Mössbauer and IR spectra. The obtained spectral parameters are available from the Supporting Information. The estimated values for the Mössbauer parameters and the observed frequencies for ν(CN) and ν(NO) vibrations in the IR spectra reproduce those results already reported for divalent transition metal nitroprussides.[33–35] Mössbauer spectra of nitroprussides reveal that the electronic structure of this family of compounds is dominated by the bonding properties of the NO group.[20]

The thermal stability of divalent transition metal nitroprussides and their behavior on the water removal on heating have already been reported.[36] In this family of compounds, the crystal water evolves below 100 °C and then the obtained anhydrous phase remains stable up to above 180 °C, except for Cu where the decomposition process begins at lower temperature, about 150 °C (see Supporting Information). Upon water removal, all of the metal interactions are concentrated on the framework

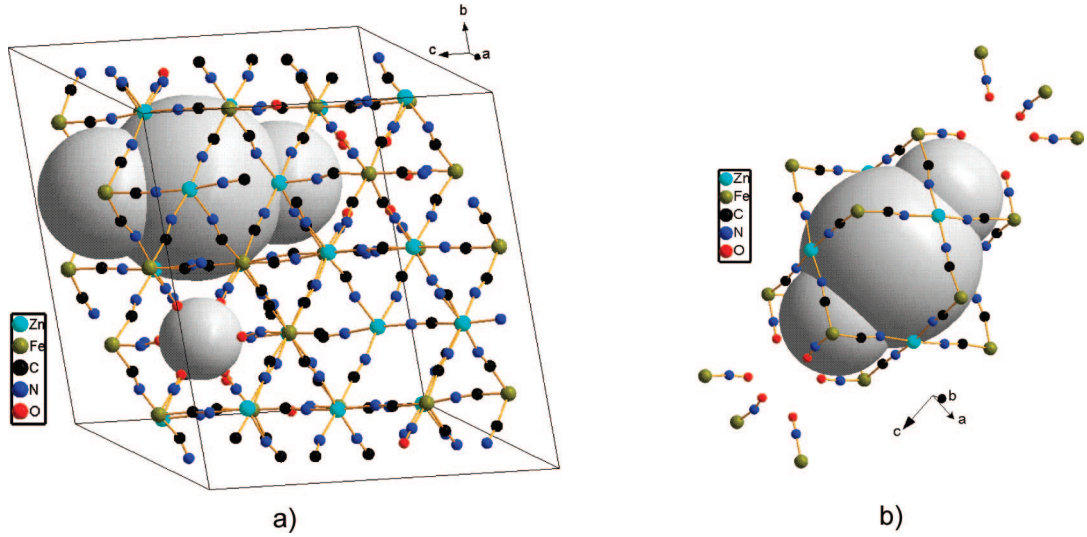

Figure 3. Relatively large ellipsoidal cavities (largest spheres), of about 15 × 7.5 Å, in anhydrous rhombohedral zinc nitroprusside communicated by the NO windows (small sphere). (a) Cavities within the unit cell. (b) An isolated ellipsoidal cavity.

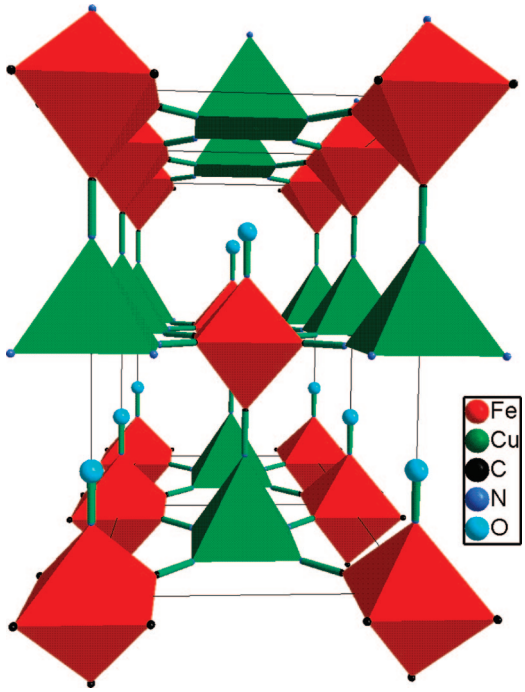

Figure 4. Structure of copper nitroprusside tetragonal (*I*4*mm*) phase. The porous network is formed by perpendicular narrow channels, one of them with a line of NO groups at its center.

ligands, the CN groups. This changes the field of forces around the metal situated at the pore surface, generating local strains that favor the fracture of microcrystals (discussed below).

$T^A_{1-x}T^B_x[Fe(CN)_5NO]\cdot xH_2O$ Series. When nitroprussides are precipitated from an aqueous solution containing two divalent transition metals, in the obtained solid the metals appear in a proportion given by the their relative affinity for the CN group at the N end. For the series prepared from equimolar mixtures of T^A and T^B, the atomic ratio found in the obtained powders is different from that in the starting solutions, 1:1 (see Table 2). The exception corresponds to copper, where no mixed compositions are usually obtained (discussed below). According to the metals atomic ratio found for this series, the metal affinity by the N end of the CN group follows the order Cu > Ni > Co > Fe > Zn > Cd > Mn. This order corresponds to the metal's ability to subtract electrons from the CN group at the N end. The ν(CN) stretching frequency in the IR spectrum can be used as a sensor of that affinity. The order of this frequency, in cm^{-1}, is Cu (2203) > Ni (2192) > Zn (2190) > Co (2188) > Fe (2179) ~ Cd (2180) > Mn (2174). The charge subtraction during the metal binding to the N atom takes place from the 5σ orbital of the CN group, which enhances the CN triple bond and raises the ν(CN) frequency.

Copper in nitroprussides shows a unique behavior with an unusual coordination to the N end. In the orthorhombic (*Amm*2) phase it is found coordinated to four equatorial CN groups and two axial waters to form a structure of layers that remain together through van der Waals type interactions, whereas in the anhydrous phase the copper atom is found with a square-base pyramidal coordination.[33] The atypical behavior of copper in cyanometallates is also found as a combined effect where the Cu^{2+} atom shows a high ability to receive an electron in its 3d hole, favoring an electronic configuration close to 3d,[10] and the CN group complements such an ability by donating electrons from its 5σ orbital, which has certain antibonding character.[37] This explains why copper corresponds to the highest observed frequency for the ν(CN) vibration in nitroprussides, 2203 cm^{-1}. In the obtained solids, copper was found forming a mixed composition only with nickel (Table 2). Nickel has the strongest polarizing power within the considered metals,[38] and as a consequence it participates in a strong interaction with the CN group. In this sense, copper and nickel show a similar behavior, and it could explain the formation of mixed copper−nickel nitroprusside.

According to the obtained XRD data (Table 1), nickel and cobalt were found to form a cubic phase with practically all the accompanying metals. This is probably due to the prevalence of these two metals in the composition of the formed solids. Manganese has a low presence in all the obtained mixed nitroprussides, and the observed structure is determined by the metal that prevails in the resulting mixed compound. The Mn−Zn combination produces a precipitate of orthorhombic (*Pnma*) structure and not the rhombohedral ($R\bar{3}$) phase observed for zinc nitroprusside. However, zinc nitroprusside is a polymorphic compound that, as a dihydrate, crystallizes with an orthorhombic unit cell (*Pnma*).[39] The behavior observed for copper was already discussed. The combination of Zn and Cd produces the orthorhombic (*Pnma*) structure where their simple nitroprussides, as dihydrates, crystallize.[39] The finding of an

TABLE 1: Unit Cell Parameters (in Å) for $T^A_{1-x}T^B_x[Fe(CN)_5NO]\cdot xH_2O$, Space Group, and Crystallite Size (S, in Å)[a]

$T^A\downarrow$ \ $T^B\rightarrow$	Mn	Fe	Co	Ni	Cu	Zn	Cd
Mn	**a = 14.112 (4)** **b = 7.511 (3)** **c = 10.542 (3)** ***Pnma***	10.338 (4) *Fm*$\bar{3}$*m* S = 472 (5)	10.267 (3) *Fm*$\bar{3}$*m* S = 440 (5)	10.192 (1) *Fm*$\bar{3}$*m* S = 331 (3)	a = 7.196 (1) b = 6.983 (1) c = 10.355 (1) *Amm*2	a = 13.995 (6) b = 7.441 (3) c = 10.528 (1) Pnma	a = 14.247 (4) b = 7.627 (1) c = 10.636 (4) Pnma
Fe	10.338 (4) *Fm*$\bar{3}$*m* S = 472 (5)	**10.337 (1)** ***Fm*$\bar{3}$*m*** **S = 1563 (6)**	10.2805 (3) *Fm*$\bar{3}$*m* S = 480 (6)	10.228 (1) *Fm*$\bar{3}$*m* S = 293 (4)	a = 7.196 (1) b = 6.983 (1) c = 10.355 (1) *Amm*2	10.378 (1) *Fm*$\bar{3}$*m* S = 453 (32)	a = 14.1553 (3) b = 7.5608 (2) c = 10.5881 (4) *Pnma*
Co	0.267 (3) *Fm*$\bar{3}$*m* S = 440 (5)	10.2805 (3) *Fm*$\bar{3}$*m* S = 480 (6)	**10.262 (1)** ***Fm*$\bar{3}$*m*** **S = 265 (4)**	10.216 (1) *Fm*$\bar{3}$*m* S = 246 (2)	a = 7.196 (1) b = 6.983 (1) c = 10.355 (1) *Amm*2	10.283 (1) *Fm*$\bar{3}$*m* S = 446 (3)	10.3045 (2) *Fm*$\bar{3}$*m* S = 382 (4)
Ni	10.192 (1) *Fm*$\bar{3}$*m* S = 331 (3)	10.228 (1) *Fm*$\bar{3}$*m* S = 293 (4)	10.216 (1) *Fm*$\bar{3}$*m* S = 246 (2)	**10.183 (1)** ***Fm*$\bar{3}$*m*** **S = 110 (3)**	10.144 (1) *Fm*$\bar{3}$*m* S = 161 (4)	10.188 (1) *Fm*$\bar{3}$*m* S = 330 (6)	10.228 (1) *Fm*$\bar{3}$*m* S = 350 (4)
Cu	a = 7.196 (1) b = 6.983 (1) c = 10.355 (1) *Amm*2	a = 7.196 (1) b = 6.983 (1) c = 10.355 (1) *Amm*2	a = 7.196 (1) b = 6.983 (1) c = 10.355 (1) *Amm*2	10.144 (1) *Fm*$\bar{3}$*m* S = 161 (39)	**a = 7.196 (1)** **b = 6.983 (1)** **c = 10.355 (1)** ***Amm*2**	a = 7.196 (1) b = 6.983 (1) c = 10.355 (1) *Amm*2	a = 7.196 (1) b = 6.983 (1) c = 10.355 (1) *Amm*2
Zn	a = 13.995 (6) b = 7.441 (3) c = 10.528 (1) Pnma	10.378 (1) *Fm*$\bar{3}$*m* S = 453 (3)	10.283 (1) *Fm*$\bar{3}$*m* S = 446 (3)	10.188 (1) *Fm*$\bar{3}$*m* S = 330 (6)	a = 7.196 (1) b = 6.983 (1) c = 10.355 (1) *Amm*2	**a = 19.304 (7)** **c = 17.625 (6)** ***R*$\bar{3}$**	a = 14.238 (1) b = 7.628 (2) c = 10.634 (3) Pnma
Cd	a = 14.247 (4) b = 7.627 (1) c = 10.636 (4) Pnma	a = 14.1553 (3) b = 7.5608 (2) c = 10.5881 (4) Pnma	10.3045 (2) *Fm*$\bar{3}$*m* S = 382 (4)	10.228 (1) *Fm*$\bar{3}$*m* S = 350 (42)	a = 7.196 (1) b = 6.983 (1) c = 10.355 (1) *Amm*2	a = 14.238 (1) b = 7.628 (2) c = 10.634 (3) Pnma	**a = 14.269 (2)** **b = 7.645 (1)** **c = 10.654 (2)** **Pnma**

[a] The crystallite size was estimated only for cubic phases.

TABLE 2: Value of x in $T^A_{1-x}T^B_x[Fe(CN)_5NO]\cdot xH_2O$

$T^A\downarrow$ \ $T^B\rightarrow$	Mn	Fe	Co	Ni	Cu	Zn	Cd
Mn	**1**	0.96	0.93	0.94	1	0.79	0.86
Fe	0.04	**1**	0.76	0.79	1	0.19	0.39
Co	0.07	0.24	**1**	0.59	1	0.14	0.11
Ni	0.06	0.21	0.41	**1**	0.55	0.15	0.10
Cu	0.0	0.0	0.0	0.45	**1**	0.0	0.0
Zn	0.21	0.81	0.86	0.85	1	**1**	0.46
Cd	0.14	0.61	0.89	0.90	1	0.54	**1**

orthorhombic (*Pnma*) structure for $Fe_{1-x}Cd_x[Fe(CN)_5NO]\cdot yH_2O$ was a nonsurprising result since iron nitroprusside, in its stable form, crystallizes in this space group.[31] The cubic structure for Fe^{2+} nitroprusside corresponds to a metastable phase, obtained using a relatively rapid crystal growth process, such as the precipitation method used here.[31]

The $(T^AT^B)-N\equiv C-Fe-C\equiv N-(T^AT^B)$ chain length, which corresponds to the cell edge (a) for the cubic phases, and the atomic ratio of T^A and T^B metals in these mixed nitroprussides, were found to be linearly correlated (Figure 5). Such a correlation is in accordance with the empirical rule known as Vegard's Law,[40] which relates the unit cell constant with the elemental composition of a solid solution or alloy. The $T-N\equiv C-Fe-C\equiv N-T$ chain length for $T = T^A$ or T^B, were estimated from the reported crystal structures for the corresponding simple nitroprussides.[31,34,39] The linear relations shown in Figure 5 indicated that the obtained mixed nitroprussides correspond to true solid solutions.

The formation of a solid solution from metals of different ionic radius generates local strains, and from that fact, the estimated values for the crystallite size in the mixed compounds were found to be smaller than those observed for simple nitroprussides (Table 1). It seems that such local strains hinder the growth of microcrystals up to a relatively large size.

This series of mixed nitroprussides was also studied from IR, Mössbauer, and TG data (see Supporting Information). The

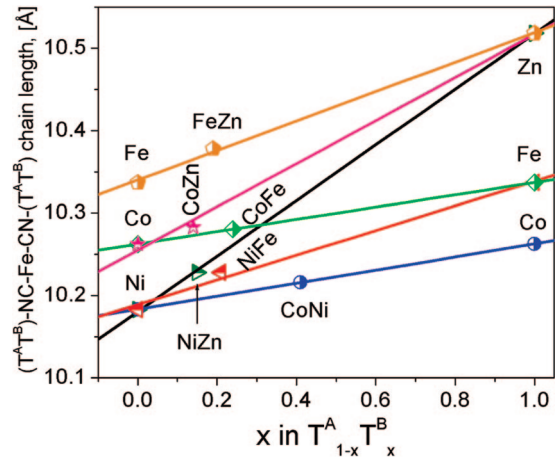

Figure 5. Linear relations between the $T-N\equiv C-Fe-C\equiv N-T$ chain length and the atomic ratio in some mixed nitroprussides. In cubic nitroprussides the unit cell edge corresponds to the $T-N\equiv C-Fe-C\equiv N-T$ chain length.

results derived from IR and Mössbauer spectroscopies are similar to those already discussed from XRD. When the two metals are found forming a mixed compound, in the IR spectrum, a single ν(CN) band with a frequency value close to that corresponding to the simple nitroprusside of the prevailing metal was observed. An analogous result was obtained from Mössbauer spectroscopy data; however, the Mössbauer parameters are even less sensitive to changes at the level of the N end. As already mentioned, the electronic structure of the building block of nitroprussides is dominated by the NO group bonding properties.[20] The effect of a mixed composition was also noted in the TG curve, particularly in the region of dehydration. A nitroprusside with a large amount of a highly polarizing metal (e.g., Ni) at the pore surface requires of a higher temperature to be dehydrated. That temperature is lower when

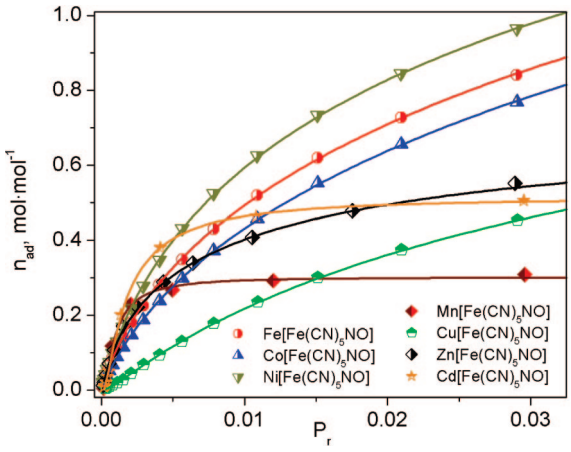

Figure 6. Carbon dioxide adsorption isotherms at 0 °C for divalent transition metals nitroprussides. The highest CO_2 adsorption capacity was observed for Ni and the lowest one for Mn. The guest−host interaction for the CO_2 molecule is modulated by the metal situated at the pore surface. The weakest guest−host interaction corresponds to Cu.

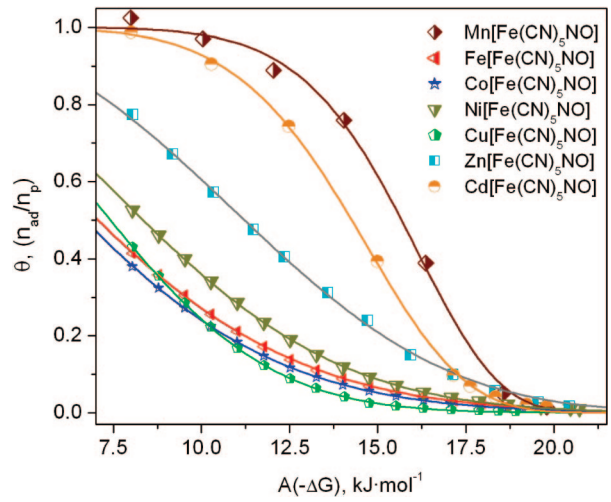

Figure 7. Characteristic curves for the CO_2 adsorption in divalent transition metal nitroprussides. For Mn and Cd, where the porous network is formed by narrow channels, the strongest guest−host interaction was found. Zn nitroprusside, where the largest cavities were observed, occupies an intermediate position probably related to the narrow access windows.

a metal such as Cd, of low polarizing power, is participating in the mixed compound.

3.2. Carbon Dioxide Adsorption Isotherms. *T[Fe(CN)$_5$NO] Series.* Figure 6 shows the CO_2 adsorption isotherms for the series of simple nitroprussides. According to these isotherms, the porous network of these compounds are accessible to CO_2. Even for Mn, Cd, and Cu with a system of particularly narrow channels, the free volume is occupied by CO_2 molecules. These isotherms also indicate that the CO_2 adsorption in the studied materials is sensitive to both the structure and the metal found at the pore surface. For a given structure, for example, cubic, the recorded isotherm shows a certain dependence on the involved metal. For Mn and Cd, both with a *Pnma* structure, such behavior is even more pronounced (Figure 6).

For Mn and Cd, the obtained isotherms saturate at particularly low values of relative pressure ($P_r < 0.01$), suggesting that the CO_2 molecule is participating in a strong interaction with the cavity's surface. The CO_2 stabilization within the free volume for the *Pnma* structure is probably dominated by the electrostatic interaction also with certain contribution from van der Waals type forces. Carbon dioxide has a quadrupole moment and, in the presence of an electric field gradient on the cavity surface, an electrostatic interaction is established. The contribution of van der Waals type interactions is related to the CO_2 molecule confinement within narrow channels. The role of the van der Waals forces for the CO_2 adsorption in this family of materials can be inferred from the obtained isotherm for copper nitroprusside. For copper, with narrow channels of the isotherm reveals a significantly weaker interaction with the channel's surface; it has the smallest slope value (Figure 6). In cyanometallates, the interaction of copper with the CN group is particularly strong, reducing the effective charge on the copper atom and its polarizing power.[37] The low effective charge on the copper atom reduces its ability for the CO_2 molecule to stabilize within the channels through electrostatic interactions. In addition, the NO group situated at only 2.9 Å from the copper atom[33] behaves as a barrier that hinders a direct metal interaction with the guest molecule. According to these features, the adsorption potential for CO_2 in copper nitroprusside must be dominated by van der Waals type interactions, which for this compound appears to be relatively weak (Figure 6).

The CO_2 adsorption in Zn (rhombohedral, $R\bar{3}$) and cubic nitroprussides (Fe, Co, Ni) can be discussed together because their cavities have similar structural features. However, some differences must be noted. Compared with the $R\bar{3}$ phase, cubic nitroprussides have a relatively smaller cavity volume but a larger porosity as a whole. For iron, for instance, the cell volume per formula unit amounts to 368 Å^3, whereas for Zn the value of this parameter is 316 Å^3. The access windows for the cubic phases are also larger than for the $R\bar{3}$ one, 4.5 versus 4 Å. These structural differences, together with the nature of the metals situated at the cavity surface, explain the higher adsorption capacity found for cubic nitroprussides in comparison with the $R\bar{3}$ phase (Figure 6). The smaller cavity size for the cubic phases favors a higher contribution of the van der Waals type interactions to the CO_2 adsorption in this subfamily. For Zn nitroprusside, this contribution must be smaller because the cavity volume is greater. All of these features explain why within these four metals (Fe, Co, Ni, Zn) the lowest CO_2 adsorption, and also the weaker guest−host interaction, corresponds to the Zn phase. The qualitative appreciation for the guest−host interaction (from the isotherm slope) within the cubic phases indicates that the adsorption potential follows the order Ni > Fe > Co. This order suggests that the CO_2 adsorption in this family is dominated by the electrostatic interaction, which for Ni, the most polarizing metal in this group, is the stronger.

The adsorption potential $A(-\Delta G)$, estimated from the experimental data according to eq 3, provides information on the guest−host interaction responsible of the CO_2 adsorption process. Figure 7 shows the characteristic curves (θ vs A) for this series of nitroprussides. For a given value of A, the fractional pore filling (θ) follows the order Mn > Cd > Zn > Ni > Fe > Co > Cu. The position of Mn and Cd with respect to the remaining metals is closely related to the confinement of the CO_2 molecule in the narrow channels of the orthorhombic (*Pnma*) structure, favoring both the electrostatic and van der Waals interactions. The high adsorption potential values observed for Zn, above those estimated for the cubic phases, could be attributed to a more localized interaction of the CO_2 molecule with the ring of six Zn atoms on the cavity surface. The order within the cubic phases (Ni > Fe > Co) parallels the reported polarizing power values for these metals,[38] corroborating that the CO_2 adsorption in this subfamily is dominated by the electrostatic interaction.

TABLE 3: Results Derived from the CO_2 Adsorption Isotherms Fitting According to the DA Model[a]

sample	E_o kJ/mol	n	n_p mol/mol	V_p cm^3/mol
$Mn[Fe(CN)_5NO]$	16.410 ± 0.121	8.0 ± 0.7	0.30 ± 0.01	12.9 ± 0.3
$Fe[Fe(CN)_5NO]$	8.645 ± 0.159	1.82 ± 0.04	2.03 ± 0.07	87 ± 3
$Co[Fe(CN)_5NO]$	8.214 ± 0.146	1.80 ± 0.04	2.02 ± 0.07	86 ± 3
$Ni[Fe(CN)_5NO]$	9.899 ± 0.122	2.15 ± 0.04	1.83 ± 0.05	78 ± 2
$Cu[Fe(CN)_5NO]$	7.85 ± 0.16	2.38 ± 0.06	1.05 ± 0.04	45 ± 2
$Zn[Fe(CN)_5NO]$	12.788 ± 0.164	2.8 ± 0.1	0.71 ± 0.02	30.4 ± 0.9
$Cd[Fe(CN)_5NO]$	15.115 ± 0.060	6.3 ± 0.2	0.51 ± 0.01	21.9 ± 0.2
$Ni_{0.94}Mn_{0.06}[Fe(CN)_5NO]$	10.1 ± 0.1	2.19 ± 0.04	1.69 ± 0.04	73 ± 2
$Ni_{0.79}Fe_{0.21}[Fe(CN)_5NO]$	9.9 ± 0.1	2.19 ± 0.05	1.56 ± 0.04	67 ± 2
$Ni_{0.59}Co_{0.41}[Fe(CN)_5NO]$	10.03 ± 0.06	2.17 ± 0.02	1.45 ± 0.02	62 ± 1
$Ni_{0.45}Cu_{0.55}[Fe(CN)_5NO]$	9.7 ± 0.1	2.07 ± 0.04	1.22 ± 0.03	52 ± 1
$Ni_{0.90}Cd_{0.10}[Fe(CN)_5NO]$	10.1 ± 0.1	2.17 ± 0.04	1.64 ± 0.04	70 ± 2
$Fe_{0.96}Mn_{0.04}[Fe(CN)_5NO]$	8.4 ± 0.2	1.79 ± 0.04	2.17 ± 0.09	93 ± 4
$Fe_{0.81}Zn_{0.19}[Fe(CN)_5NO]$	8.4 ± 0.2	1.80 ± 0.04	2.16 ± 0.08	92 ± 4
$Co_{0.93}Mn_{0.07}[Fe(CN)_5NO]$	8.3 ± 0.2	1.79 ± 0.04	2.08 ± 0.07	89 ± 3
$Co_{0.86}Zn_{0.14}[Fe(CN)_5NO]$	8.6 ± 0.2	1.83 ± 0.04	2.03 ± 0.07	87 ± 3
$Co_{0.89}Cd_{0.11}[Fe(CN)_5NO]$	8.6 ± 0.2	1.87 ± 0.05	2.12 ± 0.08	91 ± 3

[a] n_p, the limiting amount adsorbed filling the micropores; E_o, characteristic energy; n, heterogeneity parameter; V_p, pore volume.

In Table 3 the estimated values for the DA model parameters, obtained from the data fitting using a multiparameters algorithm, are collected. In this model the heterogeneity parameter (n) indicates the heterogeneity sensed by the probe molecule for the adsorption potential. A large n value corresponds to an adsorption potential with low heterogeneities. For Mn and Cd, relatively large n values of 8 and 6, respectively, were estimated (Table 3). In the narrow channels for Mn and Cd nitroprussides, all the adsorbed CO_2 molecules are sensing a same adsorption potential. All the guest molecules are interacting with the channel surface without interactions among themselves. For copper, the channels are also very narrow, favoring the CO_2 molecule interaction with only the material surface; however, the existence of a line of NO groups at the center of one of these channels introduces certain heterogeneity for the adsorption potential, and a lower n value (2.4) is obtained. The cavity geometry and the mentioned more-localized interaction of the CO_2 molecule with the Zn atoms in the $R\bar{3}$ phase are responsible for the relatively high value of n (2.8) estimated for this compound. The observed order for the estimated n values in cubic nitroprussides, Ni (2.15) > Fe (1.82) > Co (1.80), were ascribed to the strength of the guest−host interaction for the CO_2 molecule, which also follows this order. A particularly strong electrostatic interaction of the guest species with the metal situated at the pore surface reduces the relative guest−guest interaction contribution to the adsorption potential, and this is sensed as a greater n value.

The characteristic energy in the DA model (E_o) represents the average energy involved in the adsorption process. From this fact, the value of E_o can be used as a sensor for the guest−host interaction. According to the estimated E_o values (Table 3), among Mn and Cd nitroprussides, the stronger interaction corresponds to Mn, a fact already observed from the characteristic curves (Figure 7). Such behavior was attributed to the greater ability of Mn to participate in a strong electrostatic interaction with the CO_2 molecule. For the cubic subfamily (Ni, Fe, Co), the order of E_o is Ni > Fe > Co, which supports the previous discussion regarding the predominant role of the electrostatic interaction for the CO_2 adsorption in cubic nitroprussides. For copper, the smaller E_o value was found, which corresponds with the already-discussed qualitative evidence.

The smaller values estimated for pore volume within the materials under study were found for the orthorhombic phases, Mn and Cd (Table 3), and within these two metals, the small value was for Mn, which was attributed to the smaller ionic radius of the Mn^{2+} atom.[41] The cell volumes per formula unit for these two metals are 278 and 289 Å^3, respectively. It seems that the slightly higher available free space in the Cd structure is sufficient to accommodate a significantly higher amount of CO_2 molecules (Table 3). The orthorhombic unit cell contains four formula units. The maximum estimated adsorption of 0.51 mol/mol for Cd is equivalent to two CO_2 molecules per unit cell. It is probably that the CO_2 molecules are accommodated within the channels forming chains but with only a weak interaction among them. For copper, with a slightly more compact structure, 276 Å^3 per formula unit versus 278 Å^3 for Mn, for instance, the CO_2 adsorption is similar to 1.05 molecules per formula unit (2.1 molecules per unit cell). The unit cell of the $R\bar{3}$ phase contains 18 formula units and 3 cavities. This is equivalent to 4.25 CO_2 molecules per cavity. According to the reported molar volume for CO_2 (42.9 mL/mol[27]), these 4.25 molecules could be accommodated in a volume of 320 Å^3. The cavity of the $R\bar{3}$ phase has a volume above 800 Å^3. This means that the cavity is only partially occupied by CO_2 molecules, which are probably interacting with the Zn atoms (six per cavity), according to a random distribution. In such a large cavity the contribution from van der Waals forces to the CO_2 adsorption must be low. The highest ability for CO_2 adsorption was observed in cubic nitroprussides, with about six guest molecules per cell. The adsorption of these six CO_2 molecules requires a volume of at least 426 Å^3. The unit cell of this subfamily contains a large cavity with six metal centers on its surface, and with an estimated free volume of about 500 Å^3. This free space appears to be sufficient to accommodate these six CO_2 molecules through both electrostatic and dispersive interactions. The unit cell also contains smaller cavities, such as the NO cage (one per unit cell) and the interstitial voids where the CO_2 molecule could also be accommodated. However, in these smaller free spaces the adsorption potential only involves dispersive forces, and it seems that these last ones, by themselves, are insufficient to allow the CO_2 adsorption. The relatively smaller pore volume estimated for Ni, the lowest one within the cubic phases (Table 3), was attributed to a minor cavity diameter related to a strong interaction of the nickel atom with the CN group and was sensed as a small cell edge (Table 1). As already mentioned, the cell edge corresponds to the T−N≡C−Fe−C≡N−T chain length.

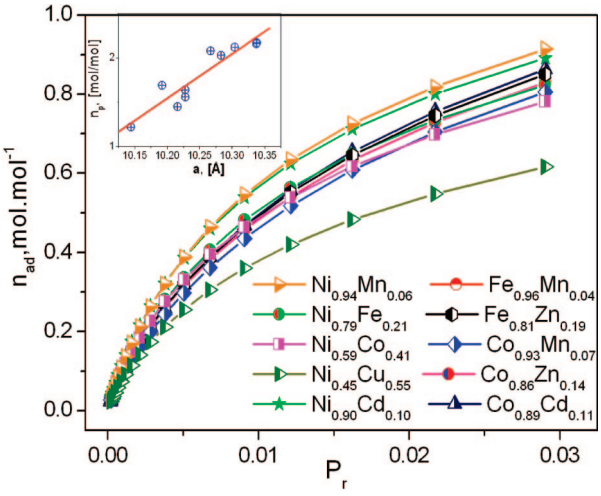

Figure 8. Carbon dioxide adsorption isotherms at 0 °C for mixed divalent transition metals nitroprussides of cubic structure. The material ability for the CO_2 stabilization within the porous framework is modulated by the metal found at the pore surface. Inset: Correlation between the maximum estimated adsorption filling the micropores (n_p) and the cell edge (a).

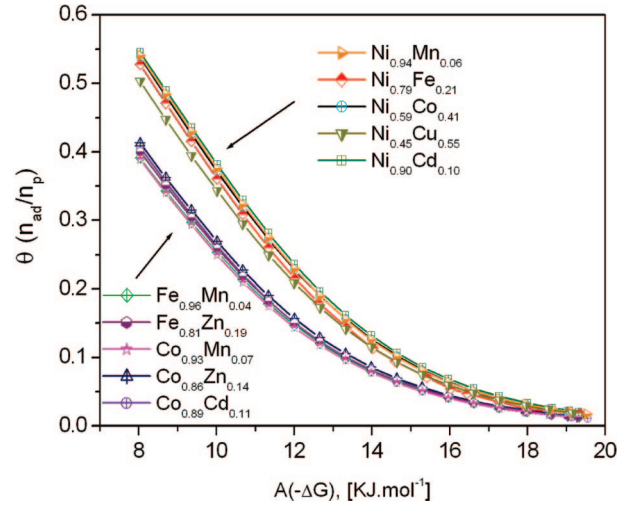

Figure 9. Characteristic curves for the CO_2 adsorption in mixed divalent transition metal nitroprussides of cubic structure. The CO_2 stabilization within the pores is dominated by the polarizing power of the metal found at the pore surface. For the Ni-containing compositions, the highest values for the adsorption work were observed.

$T^A_{1-x}T^B_x$[Fe(CN)$_5$NO] Series. The adsorption studies in mixed nitroprussides were limited to compounds of cubic structures, where in simple nitroprussides the highest adsorption capacity was observed. Figure 8 shows the CO_2 adsorption isotherms for 10 mixed compositions. These isotherms are smooth curves, without appreciable inflections, similar to those found for simple cubic nitroprussides. This suggests that the two metals are randomly distributed on the pore surface. The CO_2 molecule within the cavity senses an average adsorption potential given by a combined effect of the involved metals. The random distribution of the metals on the cavity surface was already discussed from XRD data (Table 1 and Figure 5). The participation of a metal with a large ionic radius, for example, Cd, was observed as a relatively large cell edge. In the cubic structure, where the cell edge corresponds to the T−N≡C−Fe−C≡N−T chain length, the cell edge can be used as sensor for the cavity diameter. In mixed nitroprussides, the proportion and nature of the metals on the pore surface determine both the adsorption potential and the available free volume (cavity diameter). This last effect is appreciated from Figure 8 (inset) where the existence of certain correlations among the estimated maximum adsorbed amount filling the micropores (n_p) and the cell edge for mixed cubic nitroprussides can be observed.

Conclusive evidence on the role of the metals (T) on the properties of mixed nitroprussides as microporous materials is obtained from the calculated adsorption potentials (A). Figure 9 shows the variation of the fractional pore filling (θ) with variation of the adsorption potential (A) for mixed cubic phases. All of the compositions containing nickel appear with the highest fractional pore filling (θ) for a given value of the adsorption potential, well-separated from the remaining ones to form two groups of curves. For the combination of Ni and Cu, the weakest interaction, within the Ni containing phases, was estimated. The role of the Cu atom in such behavior appears to be decisive, given by its low ability to participate in a strong electrostatic interaction with the CO_2 molecule. When in the mixed compound a metal of relatively large ionic radius (low polarizing power) prevails, for example, Fe or Co, the adsorption potential decreases (Figure 9).

In Table 3 the estimated values for the DA model parameters are reported. The higher values for the heterogeneity parameter (n), were found for the mixed compounds containing Ni. For these compounds the CO_2 molecule senses the less heterogeneous adsorption potential. The nature of such an effect was already discussed regarding nickel nitroprusside. The strong adsorption potential generated by the Ni atoms situated at the cavity surface minimizes the relative contribution of any other interaction on the guest molecule stabilization within the cavity. The inverse effect explains the low n values estimated for the remaining compositions, none containing Ni. The greater values for the characteristic energy (E_o) were also found for compounds involving Ni. That regularity agrees with the above-discussed behavior for the adsorption potential. The inverse correlation was noted for the maximum adsorbed amount filling the micropores (n_p), where the smaller values found for this parameter belong to the nickel-containing phases. The nature of this effect was already discussed in connection with the correlation shown in Figure 8 (inset).

The obtained results from the CO_2 adsorption in cubic mixed nitroprussides, and particularly the characteristic curves, contribute to support all the discussed evidence concerning the dominant role of the electrostatic interaction for the adsorption of a probe molecule, such as CO_2, with only a quadrupole moment.

3.3. Hydrogen Adsorption Isotherms. *T[Fe(CN)$_5$NO] Series.* Hydrogen storage in divalent transition metals nitroprussides has been reported for Co and Ni, with similar values for the storage capacities.[17] In this contribution the hydrogen adsorption in the remaining compositions, and also for Co and Ni, was studied. A preliminary evaluation of the hydrogen adsorption in simple cubic nitroprussides corroborates the reported results concerning a slightly higher hydrogen adsorption capacity for Ni.[17] However, compared with cobalt, nickel nitroprusside requires higher temperatures to be dehydrated, and it is usually obtained with smaller particle size.[20,34] From these last features, the hydrogen adsorption in mixed nitroprussides was limited to the cobalt-containing compositions, $Co_{1-x}T_x$[Fe(CN)$_5$NO] and to $Cu_{0.55}Ni_{0.45}$[Fe(CN)$_5$NO], this last one the only cubic phase involving copper.

Figure 10 shows the recorded isotherms for the hydrogen adsorption in simple cubic nitroprussides (Fe, Co, Ni). In Table 4 the results obtained from the fitting of these isotherms according to eq 2 are collected. The highest adsorption capacity

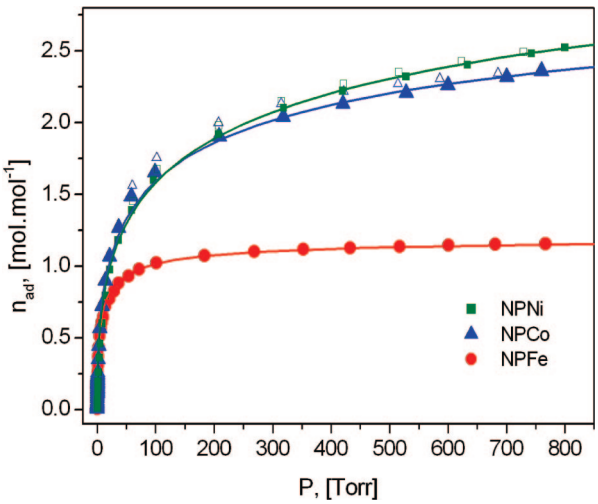

Figure 10. Hydrogen adsorption isotherms in cubic nitroprussides. The highest storage capacity was found for nickel nitroprusside. Solid symbol: adsorption; Open symbol: desorption.

was found for Ni, 2.54 mol/mol (1.85 wt %) at 75 K and 850 Torr. This is equivalent to 7.62 H_2 molecules per unit cell. This value is ~10% higher than that already reported for this compound.[17] Such difference could be ascribed to the use of different sample preparation conditions. We have noted that the hydrogen adsorption results are very sensitive to the sample preparation and activation. For a same family of porous compounds different groups have reported storage capacities with even higher differences for similar compositions.[14,15,42] Cubic nitroprussides have a large cavity, ca. 8.5 Å in diameter, per unit cell. The 7.62 H_2 molecules adsorbed per unit cell estimated for Ni are probably accommodated within that large cavity where the hydrogen molecule could be stabilized through electrostatic interactions between its quadrupole moment and the cavity electric field gradient, without discarding some direct interaction with the metal located at the cavity surface. In the remaining free spaces, the NO-bound cage, and interstitial voids, H_2 must be stabilized through dispersive interactions. The above-discussed results from the CO_2 adsorption suggest that the electrostatic interaction could also be the dominant driving force for the hydrogen adsorption. For $T[Pt(CN)_6]$, a family of compounds with only interstitial voids, no H_2 adsorption has been reported.[15] No hydrogen adsorption has also been reported for anhydrous $Mn_2[Fe(CN)_6]$,[18] a compound with only interstitial free spaces.[43] However, from a neutron diffraction study in $Cu_3[Co(CN)_6]_2$, the H_2 adsorption in interstitial positions has been reported.[16] In this last compound, with a greater number of vacancies of the building block than cubic nitroprussides, 33 versus 25% of the available structural sites in the unit cell, respectively, the interstitial voids adjacent to a vacancy could also be able for the H_2 stabilization within the solid through electrostatic interactions.

For iron a significantly smaller maximum adsorption was observed, about 1.26 mol/mol, equivalent to 3.78 H_2 molecules per unit cell (0.95 wt %). Such low adsorption capacity for iron was not observed for the CO_2 adsorption. This reduction in storage capacity could be attributed to a combined effect of two factors: (a) a lower ability of the cavity for the hydrogen molecule stabilization and (b) the occurrence of structural changes in the studied sample due to the prolonged heating time under vacuum. Reported studies on hydrogen adsorption in Prussian blue analogues have revealed certain dependence of the H_2 storage capacity on the metal situated on the pore surface.[14,15] Regarding iron nitroprusside sample stability, an XRD powder pattern taken at the end of the H_2 adsorption experiment shows significant peaks broadening. This was interpreted as evidence of a fracture process of their crystallites to form a material of lower crystalline order and, probably, also to partial sample decomposition (see Supporting Information). IR spectra recorded at the end of the H_2 adsorption experiment revealed the appearance of a weak ν(CN) band at 2080 cm^{-1}, attributed to the loss of the NO group. In nitroprussides the decomposition process is sensed as the loss of NO groups.[44]

Figure 11 shows the recorded H_2 adsorption isotherms for noncubic nitroprussides. For copper, no hydrogen adsorption was observed. This behavior is consistent with the above-discussed results for the CO_2 adsorption in copper nitroprusside. The porous network of this compound is quite similar to that of $T[Pt(CN)_6]$, which is formed by only interstitial spaces, where no hydrogen adsorption is observed.[15] It seems that the van der Waals interaction, by itself, is insufficient to allow the H_2 adsorption in porous cyanometallates. For Mn, Zn, and Cd, the obtained H_2 adsorption isotherms show evidence of kinetic effects, which are more pronounced in manganese nitroprusside. From intermediate pressure values a systematic increase for the adsorbed quantity, even for large measurement times of up to two weeks per isotherm, is observed. The presence of kinetic effects is usually appreciated by an adsorption curve free of saturation in the region of intermediate to higher pressures, indicating that the adsorbed amount is determined by the chemical potential, when the diffusion through the windows is favored by a higher availability of adsorbate molecules. Such evidence was observed in the recorded H_2 adsorption isotherms for these three nitroprussides. Conclusive evidence on the occurrence of kinetic effects for these compositions was obtained by recording isotherms for different equilibrium intervals after the H_2 dosing. Figure 12 shows two of such isotherms for the case of Mn. In addition, the adsorption process appears to be nonreversible. The desorption curve is quite different from the adsorption one. For Zn the observed kinetic effects are probably related to the small size for the pore windows, of ca. 4 Å, which are delimited by six NO groups. For Mn and Cd, the dominant factor in the observed behavior could be a strong interaction between the hydrogen molecule and the pore surface where metal centers with unsaturated coordination environments are found. Such an interaction probably reduces the hydrogen diffusion rate through the channels system, hindering an appropriate filling of the available free space with H_2 molecules. This agrees with the strong kinetic effects observed for Mn, the most polarizing metal within orthorhombic phases (Mn, Cd).

For cobalt and nickel nitroprussides the hydrogen adsorption heats have been reported to be 6.5 and 7.5 kJ/mol, respectively.[17] The larger ΔH_{ads} value is found for the metal of stronger polarizing power (Ni) at the pore surface, which agrees with the above-discussed qualitative discussion on the role of the electrostatic interaction as the main driving force for the hydrogen adsorption in the materials under study. We also have estimated the H_2 adsorption heats for cobalt nitroprusside from eq 3 and adsorption isotherms recorded at 75 and 85 K (see Supporting Information), and a slightly higher value was obtained, of about 8.5 kJ/mol (Figure 13) at low coverage, when the guest−guest interactions can be ignored. The adsorption heat value decreases with the increase of the adsorbed amount, an expected behavior due to a weaker effect of the cavity surface.

$Co_{1-x}T_x[Fe(CN)_5NO]$ Series. Figure 14 shows the hydrogen adsorption isotherms for this mixed series. In Table 4 the results obtained from the fitting of these isotherms according to eq 2

TABLE 4: Results Derived from the H_2 Adsorption Isotherms Fitted According to the Langmuir−Freundlich Model [a]

compound	temp. [K]	n_p [mol/mol]	H_2/cavity	g	wt %
$Ni[Fe(CN)_5NO]$	75	4.27 ± 0.2	12.8 ± 0.2	2.4 ± 0.1	3.11 ± 0.02
$Co[Fe(CN)_5NO]$	75	3.5 ± 0.2	10.5 ± 0.2	2.2 ± 0.1	2.54 ± 0.02
	85	3.4 ± 0.1	10.2 ± 0.1	1.87 ± 0.08	2.27 ± 0.01
$Fe[Fe(CN)_5NO]$	75	1.26 ± 0.01	3.8 ± 0.01	1.8 ± 0.1	0.93 ± 0.01
$Co_{0.93}Mn_{0.07}[Fe(CN)_5NO]$	75	3.9 ± 0.1	11.7 ± 0.1	2.1 ± 0.1	2.83 ± 0.01
	85	3.25 ± 0.05	9.75 ± 0.05	1.67 ± 0.04	2.36 ± 0.05
$Co_{0.41}Ni_{0.59}[Fe(CN)_5NO]$	75	3.29 ± 0.09	9.9 ± 0.09	2.2 ± 0.2	2.39 ± 0.09
$Co_{0.86}Zn_{0.14}[Fe(CN)_5NO]$	75	2.33 ± 0.02	7.0 ± 0.02	1.0 ± 0.2	1.69 ± 0.02
$Co_{0.89}Cd_{0.11}[Fe(CN)_5NO]$	75	1.92 ± 0.08	5.3 ± 0.08	1.9 ± 0.4	1.37 ± 0.4
$Ni_{0.45}Cu_{0.55}[Fe(CN)_5NO]$	75	0.96 ± 0.01	2.8 ± 0.01	1.55 ± 0.3	0.67 ± 0.01

[a] n_p is the limit capacity of micropores, g is the osmotic coefficient, H_2/cavity is the estimated limit amount of H_2 molecules per cavity, and wt % is the maximum estimated adsorption in weight percent.

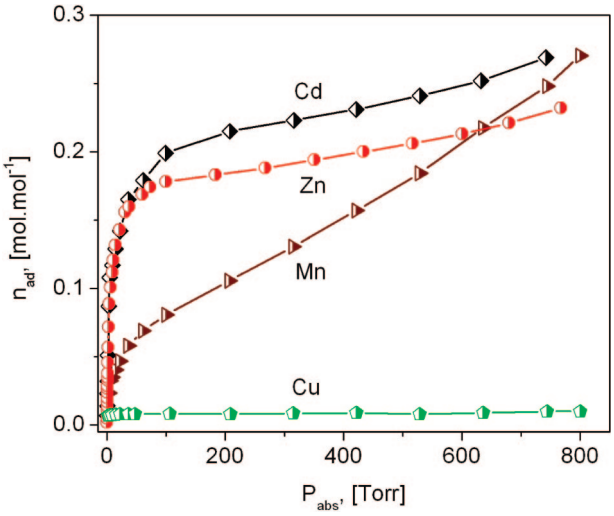

Figure 11. Hydrogen adsorption isotherms for noncubic nitroprussides (Mn, Cu, Zn, and Cd). For Cu no hydrogen adsorption was detected. For Mn, Zn, and Cd the obtained isotherms show an increasing slope in the higher pressure region that was attributed to kinetic effects (see Figure 12).

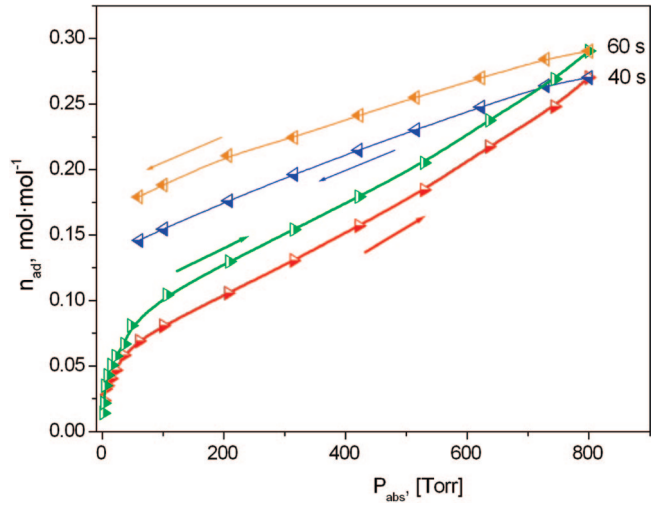

Figure 12. Kinetic effects for the hydrogen adsorption in Mn^{2+} nitroprusside. The obtained adsorption curve shows a nonreversible behavior and has a pronounced dependence on the equilibrium time after dosing. The equilibrium time after dosing is indicated. Such behavior was ascribed to the combined effect of narrow pore windows and a strong interaction of the hydrogen molecule with the channels surface that reduces the diffusion rate.

are collected. These isotherms show a definite dependence on the metal (T) accompanying cobalt in this series. The accompanying metal modulates the volume of the larger cavity, the windows size, and also the electric field gradient that the hydrogen molecule senses within that region. The observed modulating effect of the metal on these isotherms results from the contribution of at least these three factors. As already mentioned, the electronic structure of nitroprussides is dominated by the NO group. From this fact, no simple correlation among the nature and amount of the T metal at the pore surface and the maximum H_2 adsorption can be established. The largest n_p value (maximum adsorption) was observed for Mn. The larger ionic radius for Mn^{2+}, compared to Co^{2+}, [41] leads to a slight increase for the cavity volume and the cavity windows size when some cobalt atoms are replaced by manganese at the cavity surface. These two facts could explain the observed increase for the H_2 adsorption capacity in $Co_{0.93}Mn_{0.07}[Fe(CN)_5NO]$ relative to simple cobalt nitroprusside. For this compound, the involved adsorption heat was estimated, and no difference regarding the simple composition was found (Figure 13). At the opposite position of this series $Cd_{0.11}Co_{0.89}[Fe(CN)_5NO]$ is found. Because in this case the cavity volume is even larger, the smaller n_p value was attributed to the effect of the Cd atom on the adsorption potential for H_2 molecules. Within the considered metals, the greater ionic radius corresponds to Cd,

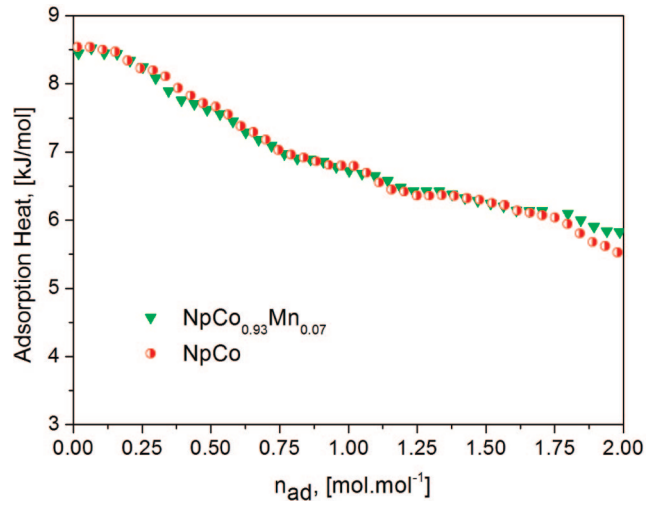

Figure 13. Hydrogen adsorption heat for Co and Co−Mn nitroprussides.

and from this fact, it has the lower polarizing power and contributes the reduction of the electric field gradient at the cavity.

For all studied samples of cubic nitroprussides, slight kinetic effects for the H_2 adsorption were observed, even for large

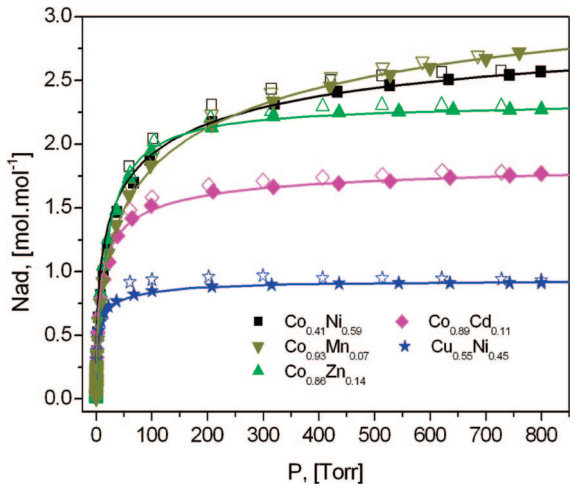

Figure 14. Hydrogen adsorption isotherms in $Co_{1-x}T_x[Fe(CN)_5NO]$ and $Cu_{0.55}Ni_{0.45}[Fe(CN)_5NO]$. The highest storage capacity was found for cobalt−manganese nitroprusside. For all the studied samples slight kinetic effects were observed, even for large equilibrium time. Solid symbol: adsorption; open symbol: desorption.

equilibrium intervals (60 s) up to a week of measurement time. Such behavior was attributed to the large polarizing power of the NO group, which deforms the environment of the iron atom in the $[Fe(CN)_5NO]$ unit. The average $C_{eq}-Fe-C_{eq}$ angle (C_{eq} represents equatorial carbons) in cubic nitroprussides is ~170°.[20,34] In addition, the environment of the outer metal is also distorted; on average, $N_{eq}-T-N_{eq}$ (N_{eq} represents equatorial nitrogens) is ~177°.[20,34] These local distortions reduce the effective cavity windows size and the H_2 diffusion rate. For Prussian blue analogues where the H_2 adsorption has been studied, also with a cubic (Fm3m) structure but practically free of such local distortions, the occurrence of kinetic effects in the obtained data has not been reported.[14,15,18,19]

Role of the Metal on the H_2 Adsorption Potential. In the LF model used to evaluate the H_2 adsorption data, the estimated value for the osmotic coefficient (g) represents a sensor for the strength of the guest−host interaction.[45] We have found that this parameter is particularly useful in comparative studies for the H_2 storage in a given family of materials.[29] For $g = 1$, eq 2 is equivalent to the Langmuir model, which supposes a mobile adsorbate without lateral interactions among the adsorbate particles, with all of them sensing the same adsorption potential.[46] A value of $g > 1$ represents a deviation from such ideal conditions. When the value of g for the adsorption isotherms recorded at 75 and 85 K are compared, the larger g values correspond to the former (Table 4). This behavior confirms the interpretation given to the value of g. At a lower adsorption temperature, the H_2 molecule senses a stronger adsorption potential, and a more localized adsorption is expected. Corresponding with the reported adsorption heats for NPNi and NPCo,[17] the estimated g value for Ni is slightly greater than for Co, 2.4 vs 2.2. A metal at the cavity surface with a higher polarizing power leads to a stronger interaction for H_2 with the cavity surface. According to the value of g and within the mixed compositions containing Co, the order for the strength of the guest-interaction is Ni > Mn > Cd > Zn (Table 4). Except for Zn, this is the order of these metals according to their polarizing power.[38] For $NPNi_{0.45}Cu_{0.55}$ the smaller g value (1.55) was found (Table 4), which was attributed to the above-discussed bonding interaction properties of copper with the CN group, which reduces the effective charge on the copper atom and its polarizing power.

The H_2 coordination to the metal centers located at cavity surface supposes the stabilization of that bond through an electron back-donation from the metal t_{2g} orbitals to the σ^* orbitals of the hydrogen molecule.[47] Divalent transition metals have a relatively low electron density to favor that back-donation effect. However, a direct interaction of H_2 with the metal in this family of materials can not be discarded, particularly for those metals with a high ability to subtract charge from the CN groups.

Conclusions

The hydrogen adsorption in divalent transition metal nitroprussides was found to be dominated by the electrostatic interaction between the H_2 molecule quadrupole moment and the pore electric field gradient. For Cu with only interstitial voids, no hydrogen adsorption was observed. In porous structures with narrow channels (Mn, Zn, Cd), the electrostatic interaction and the narrow channels system are responsible for the pronounced kinetic effects observed in the recorded adsorption isotherms. The highest adsorption capacities were found for cubic phases where the larger available free volume is combined with an appropriate adsorption potential within the cavity. Such an adsorption potential is determined by the metals found at the cavity surface and it can be modulated from the combination of different metals. This family of compounds forms true solid solutions where the obtained structure is determined by the metal that prevails in the composition of the formed solid. For the adsorption of CO_2, no kinetic effects were observed. This was attributed to the small cross section for this molecule along O−C−O axis. The CO_2 adsorption in the studied solids is also dominated by the electrostatic interaction between the carbon dioxide quadrupole moment and the cavity electric field gradient.

Acknowledgment. L.R. acknowledges the support provided by the ALFA Project NANOGASTOR for her PhD studies. The help of J. Rodríguez-Hernández and M. Avila-Santos for the preparation of some illustrations is highly appreciated. This research was partially supported by the Projects SEP-2004-C01-47070, SEP-CONACyT-2007-61541, and DGAPA IN-115708. The authors thank E. Fregoso-Israel from IIM-UNAM for the TG data collection and J.C. Llópiz by the facility for the CO_2 adsorption data acquisition in ASAP 2010 equipment. The access to Laboratorio Nacional de Luz Síncrotron (LNLS) at Campinas, Brazil is greatly recognized.

Supporting Information Available: Supplementary structural information (XRD, IR, Mössbauer, and TG) and adsorption data are available free of charge via the Internet at http://pubs.acs.org.

References and Notes

(1) Schlapbach, L.; Züttel, A. *Nature* **2001**, *414*, 353, and references therein.
(2) U.S. Department of Energy, Energy Sources, Hydrogen, http://www.energy.gov/energysources/hydrogen.htm.
(3) Chen, P.; Xiong, Z., J.; Luo, J.; Lin, J.; Tan, L. K. *J. Phys. Chem. B* **2003**, *107*, 10967.
(4) Chen, P.; Xiong, Z., J.; Luo, J.; Lin, J.; Tan, L. K. *Nature* **2002**, 420–302.
(5) Janot, R.; Eymery, J.B.; Tarascon, J.M. *J. Phys. Chem. C* **2007**, *111*, 2335.
(6) Torres, F. J.; Vitillo, J. G.; Civalleri, B.; Ricchiardi, G.; Zecchina, A. *J. Phys. Chem. C* **2007**, *111*, 2505.
(7) Naab, F.U.; Dhoubhadel, M.; Gilbert, J. R.; Savage, L. K.; Holland, O. W.; Duggan, J. L.; McDaniel, F. D. *Phys. Lett. A* **2006**, *352*, 152.
(8) Bhatia, S. K.; Myers, A. L. *Langmuir* **2006**, *22*, 1688.

(9) Kazansky, V. B.; Borovkov, V. Y.; Karge, H. G. *Micropor. Mesorpor. Mater.* **1998**, *22*, 251.
(10) Zecchina, A.; Bordiga, S.; Vitillo, J. G.; Ricchiardi, G.; Lamberti, C.; Spoto, G.; Bjorgen, M.; Lilleruk, K. P. *J. Am. Chem. Soc.* **2005**, *127*, 6361.
(11) Rosi, N. L.; Exkert, J.; Eddaoudi, M.; Vodak, D. T.; Kim, J.; O'Keeff, M.; Yaghi, O. M. *Science* **2003**, *300*, 1127.
(12) Zhao, X.; Xiao, B.; Fletche, A. J.; Thomas, K. M.; Bradshaw, D.; Rosseinsky, J. *Science* **2004**, *306*, 1012.
(13) Kitagawa, S.; Kitaura, R.; Noro, S. I. *Angew. Chem., Int. Ed.* **2004**, *43*, 2334.
(14) Kaye, S. S.; Long, J. R. *J. Am. Chem. Soc.* **2005**, *127*, 6506.
(15) Chapman, K. W.; Southon, P. D.; Weeks, C. L.; Kepert, C. J. *Chem. Commun.* **2005**, 3322.
(16) Hartman, M. R.; Peterson, V. K., Y.; Liu, Y.; Kaye, S. S.; Long, J. R. *Chem. Mater.* **2006**, *18*, 3221.
(17) Culp, J. T.; Matranga, C.; Smith, M.; Bittner, E. W.; Bockrath, B. *J. Phys. Chem. B.* **2006**, *110*, 8325.
(18) Kaye, S. S.; Long, J. R. *Catal. Today* **2007**, *120*, 311.
(19) Natesakhawat, S.; Culp, J. T.; Matranga, C.; Bockrath, B. *J Phys. Chem. C* **2007**, *111*, 1055.
(20) Balmaseda, J.; Reguera, E.; Gomez, A.; Roque, J.; Vazquez, C.; Autie, M. *J. Phys. Chem. B* **2003**, *107*, 11360.
(21) Chen, B.; Ockwing, N. W.; Millward, A. R.; Contreras, D. S.; Yaghi, O. M. *Angew. Chem., Int. Ed.* **2005**, *44*, 4745.
(22) Louer, D.; Vargas, R., J. *Appl. Crystallogr.* **1982**, *15*, 542.
(23) Guinier, A., *X-Ray Diffraction*; Dover Publications: Mineola, New York, 1994.
(24) Dubinin, M. M., In *Progress in Surface Science and Membrane Science*; Cadenheat, D. A. Ed.; Academic Press: New York, 1975.
(25) Bering, B. P.; Serpinskii, V. V. *Izv. Akad. Nauk SSSR, Ser. Khim.* **1974**, *11*, 2427.
(26) Balmaseda, J.; Reguera, E.; Rodríguez-Hernández, J.; Reguera, L.; Autie, M. *Micropr. Mesopor. Mater.* **2006**, *96*, 222.
(27) Stoeckli, F. *Russ. Chem. Bull., Int. Ed.* **2001**, *50*, 2265.
(28) Roque-Malherbe, R. *Micropor. Mesopor. Mater.* **2000**, *41*, 227.
(29) Reguera, L.; Balmaseda, J.; del Castillo, L. F.; Reguera, E. *J. Phys. Chem. C* **2008**, *112*, 5589.
(30) Rouquerol, F., Rouquerol, J.,Sing, K. *Adsorption by Powders and Solids: Principles, Methodology and Applications*; Academic Press: London, 1999.
(31) Reguera, E.; Dago, A.; Gómez, A.; Fernández, J. *Polyhedron* **1996**, *15*, 3139.
(32) Mullica, D. F.; Sappenfield, E. L.; Tippin, D. B.; Leschnitzer, D. H. *Inorg. Chim. Acta* **1989**, *164*, 99.
(33) Gomez, A.; Rodríguez-Hernández, J.; Reguera, E. *J. Chem. Crystall.* **2004**, *34*, 893.
(34) Gomez, A.; Rodríguez-Hernández, J.; Reguera, E. *Powder Diffract.* **2007**, *22*, 27.
(35) Rodríguez-Hernández, J.; Reguera, E.; Mir, M.; Mascarenhas, Y. P. *Powder Diffract.* **2007**, *22*, 40.
(36) Torres, E.; Balmaseda, J.; del Castillo, L. F.; Reguera, E. *J. Therm. Anal. Calorim.* **2006**, *86*, 371.
(37) Reguera, E.; Rodríguez-Hernández, J.; Champi, A.; Duque, J. G.; Granados, E.; Rettori, C. *Z. Physik. Chem.* **2006**, *220*, 1609.
(38) Zhang, Y. *Inorg. Chem.* **1982**, *21*, 3886.
(39) Gomez, A.; Reguera, E.; Lanchan, C. *Polyhedron* **2001**, *20*, 165.
(40) Denton, A. R.; Ashcroft; N.W, *Phys. Rev. A* **1991**, *43*, 3116.
(41) Shannon, R. D. *Acta Crystallogr. A* **1976**, *32*, 751.
(42) Kaye, S. S.; Dailly, A.; Yaghi, O. M.; Long, J. R. *J. Am. Chem. Soc.* **2007**, *129*, 14176.
(43) Rodríguez-Hernández, J.; Gómez, A.; Reguera, E. *J. Phys. D: Appl. Phys.* **2007**, *40*, 6076.
(44) Reguera, E.; Balmaseda,Rodríguez-Hernández, J.; Autie, M.; Gordillo, A.; Yee-Madeira, H. *J. Por. Mater.* **2004**, *11*, 219.
(45) Yakubov, T. S.; Bering, B. P.; Dubinin, M. M.; Serpinskii, V. V. *Izv. Akad. Nauk SSSR, Ser. Khim.* **1977**, 463.
(46) Roque-Malherbe, R., In *Adsorption and Diffusion in Nanoporous Materials*; CRC Press, Taylor & Francis Group: Boca Raton, London, New York, 2007.
(47) Kubas, G. J. *Chem. Rev.* **2007**, *107*, 4152.

JP801955P